nature communications

Article

https://doi.org/10.1038/s41467-025-62270-3

The mechanotransducer Piezo1 coordinates metabolism and inflammation to promote skin growth

Received: 5 September 2024

Accepted: 14 July 2025

Published online: 25 July 2025

Check for updates

Yingchao Xue[1] ✉, Elizabeth Winnicki[1], Zhaoxu Zhang[1], Ines Lopez[1], Saifeng Wang[1], Charles Kirby[1], Sam S. Lee[1], Ang Li[1], Chaewon Lee[1], Hana Minsky[1], Kaitlin Williams[1], Kevin Yueh-Hsun Yang[2], Ling He[3], Sashank K. Reddy[2,4,5] ✉ & Luis A. Garza[1,6,7] ✉

The skin has a remarkable ability to grow under constant stretch. Using a controlled tissue expansion system in mice, we identified an enhanced inflammatory-metabolic network in stretched skin via single-cell RNA sequencing, flow cytometry and spatial transcriptomics. Stretched epidermal cells exhibit heightened cellular crosstalk of CXCL, CCL, TNF, and TGF-β signaling. Additionally, skin expansion increases macrophage and monocyte infiltration in the skin while altering systemic immune cell profiles. Glycolysis-related genes, including Glut1 and Aldoa were significantly elevated. We hypothesize that Piezo1, a non-selective calcium-permeable cation channel, senses tension in stretched skin, driving these responses. The epidermal-Piezo1 loss-of-function animals show reduced skin growth, tissue weight, tissue thickness, macrophage infiltration, and glycolysis activity. Conversely, animals with a pharmacological Piezo1 gain of function exhibit an increase in these factors. Our findings highlight the coordinating role of Piezo1 for metabolic changes and immune cell infiltration in tension-induced skin growth.

As the boundary between the organism and the outside world, the skin must respond constantly to internal and external mechanical stimuli. Excessive mechanical stress can lead to harmful changes in the skin's structure, while moderate tension can promote skin growth within a healthy range. For example, physiological stretch and growth of the skin occur during development, growth into adulthood, and in pregnancy[1]. Pathophysiologic skin growth also occurs during obesity and constitutes a significant burden in patients who subsequently undergo significant weight loss. The growth capacity of skin is also harnessed clinically for reconstructive purposes in a process called tissue expansion (TE)[2,3]. During TE, surgeons place a balloon underneath the skin and inject saline to enlarge it, causing the skin to grow over time (3–5 months)[4,5]. This model of skin growth differs from wounding or hair regeneration models[6], as it primarily reflects how mechanical stretching leads to the proliferation of keratinocytes and the formation of supportive structures such as blood vessels. The newly generated skin can then be moved to areas that need coverage. This is required in trauma repair, nevus resection, scalp reconstruction, or breast reconstruction after surgery. However, the extended duration of expansion and the risk of infection during this process are problematic[7–9]. Furthermore, the mechanism underlying tension-induced skin growth is unclear. Defining this mechanism will afford insights into organ size

[1]Department of Dermatology, Johns Hopkins University, Baltimore, MD, USA. [2]Department of Plastic and Reconstructive Surgery, Johns Hopkins University, Baltimore, MD, USA. [3]University of Arizona College of Medicine-Phoenix, Phoenix, AZ, USA. [4]Department of Biomedical Engineering, Johns Hopkins University, Baltimore, MD, USA. [5]Institute for NanoBioTechnology, Johns Hopkins University, Baltimore, MD, USA. [6]Department of Cell Biology, Johns Hopkins University, Baltimore, MD, USA. [7]Department of Oncology, Johns Hopkins University, Baltimore, MD, USA. ✉e-mail: yxue8@jhmi.edu; sreddy6@jhmi.edu; lag@jhmi.edu

control and may yield more effective therapeutics to create new skin potentially without the need for expanders[10].

Our previous transcriptomic analyses suggested alterations in metabolic and inflammatory pathways during tissue expansion[11]. We generally categorized stretch-regulated pathways in the skin; microarray and epidermal single-cell sequencing demonstrated enriched terms including metabolic processes, cellular response to cytokine stimuli, and hypoxia[11]. These observations are consistent with other studies emphasizing the importance of reprogramming glucose metabolism in tissue restoration[12]. In glucose metabolism, glycolysis initiates catabolic metabolism to fuel cell proliferation and tissue repair during regeneration. In a skin injury model in mice, for example, keratinocytes increase glycolytic activity, a key requirement for effective wound healing[13]. Another study has demonstrated that injury triggers glycolysis during zebrafish adult tail-fin regeneration, which is crucial for osteoblast dedifferentiation, proliferation, blastema formation, and tail-fin regeneration[14]. These findings highlight the critical connection between glycolysis and skin restoration, raising the question of what upstream regulators link injury to modified metabolism.

In addition to metabolic changes, immune cell activation is crucial for tissue restoration and cell fate determination in skin[15,16]. Inflammatory signals, such as chemokines and cytokines, are essential for supporting tissue repair[17,18]. Coordinated communication between immune cells and local skin stem cells is vital, and failure in this coordination may lead to chronic inflammation and pathological fibrosis[19]. Interestingly, recent studies by our group and others demonstrate that inflammation occurs with skin stretch[20–22], with less information available regarding the specific changes in immune cell types and their impact on TE. Thus, gaining a better understanding of these processes could reveal important biological mechanisms related to TE and help promote skin growth. However, how tension is sensed in the skin to drive inflammatory and metabolic changes is not known. An important question is to define the factor that triggers these changes.

One such candidate factor would be a mechanotransducer in keratinocytes sensitive to external physical stimuli. Piezo proteins, including Piezo1 and Piezo2, are evolutionarily conserved mechanosensitive calcium-permeable cation channels that play a crucial role in converting mechanical force into electrochemical signals[23]. Piezo1 is abundantly expressed in the skin, while Piezo2 is more prevalent in dorsal root ganglion (DRG) neurons[23]. In keratinocytes, Piezo1 modulates cutaneous mechanosensation[24], while in hair follicles mechanically compressed stem cells undergo calcium-dependent apoptosis through the Piezo1-TNFα signal[25]. These findings suggest the functional roles of Piezo1 in skin mechanosensation. In our tissue expansion model, we observed an increased calcium ion binding signal in the skin after tissue expansion[11]. Additionally, the top two upregulated genes from single-cell sequencing, *S100A8* and *S100A9*[11], are associated with calcium signals[26]. Given this evidence from our work and others, we hypothesize that the calcium-permeable cation channel Piezo1 functions as an upstream mechanotransducer to coordinate necessary downstream biological activity to induce organ growth during tissue expansion.

In summary, the functional data on PIEZO1 for a role in both metabolism and immunity suggest the need for more study to define a physiological context where these functions might be relevant. A unified coherent model where PIEZO coordinates inflammation, metabolism, and mechanosensing in a single response is missing. Here, we discovered that mechanosensing through Piezo1 mediates such coordination in tension-induced skin growth through an inflammatory-metabolic network. These results advance our understanding of tension-induced skin growth and suggest promising avenues for innovative therapeutic strategies in wound healing and tissue engineering.

Results

A mouse model of tissue expansion

We developed a mouse model of tissue expansion to study the cellular and molecular mechanisms involved in tension-induced skin growth. A miniaturized silicone tissue expander is placed under the back skin and gradually inflated with saline injection through a remote port leading to substantial skin growth (Fig. 1A, B). Samples are collected following the completion of all injections starting at PI-0 (day 0 post-complete injection), PI-14, PI-32, and PI-70 time points after the tissue expansion. We use non-expanded (NE) controls to compare changes in tissue weight and histology (Fig. 1A). Our findings show that the expanded skin increased in size and weight over time as compared to the NE controls (Fig. 1B, C). Histologically, we observed thickening of the expanded skin's epidermis, while the thickness of the dermis did not change significantly (Fig. 1D).

Spatial transcriptomics unveils a stretch-induced bio-program

To examine specific pathway changes within the entire skin at both the spatial and single-cell level, we gathered expanded (E) and non-expanded (NE) control samples for a multi-panel in situ spatial transcriptomics (xenium; 10x Genomics). Spatial clustering revealed 6 groups of cells organized in the bilaminar skin, including the suprabasal, basal, hair follicle (HF), sebaceous gland (SG), dermal cells (including fibroblasts and endothelial cells in the dermis), and immune cells (Fig. 1E, F, Fig. S1). We then compared how the relative amounts of each population changed during expansion. The fractions of basal and suprabasal cells increased after expansion, indicating robust growth (Fig. 1G). Meanwhile, there was a decrease in HF and SG cells, consistent with our previous findings of a lack of hair follicle neogenesis during epidermal area expansion (Fig. 1G). Finally, we observed elevated infiltration of immune cells in the skin, suggesting a tension-induced skin inflammatory response (Fig. 1G).

Based on our previous publication and literature precedent, we curated a top list of genes that show significant induction, which we named as stretch-induced signature genes[11,20]. We assessed these transcripts spatially on the Xenium assay. We calculated the stretch signature score depending on this list and found significant increase of this pathway score in the E skin samples across various cell types (Fig. 1H). Within this pathway, We identified several genes correlating to skin expansion, such as *Akt1*, *Itgb1* and *Myh9*, which sense mechanical stress in the skin niche[11,20], were significantly higher in expanded cell groups of basal, HF, dermal, and immune cells (Fig. 1I). Additionally, the gene *Postn*, which is linked to mechanical sensing and restoration[27], displayed a tension-induced pattern in epidermal keratinocytes, dermal fibroblasts, and immune cells (Fig. 1I). Some genes exhibited differences between epidermal and dermal cells. For instance, *S100a8*, *Stfa1*, and *Sprr2a3* were significantly elevated in epidermal cells with robust expression, but not in dermal and immune cells (Fig. 1I).

In our previous microarray data analysis, we found enrichment of the hypoxia pathway in expanded skin[11]. In the xenium assay, we assessed a list of genes related to angiogenesis and found that this pathway is significantly elevated in the expanded skin cell groups, indicating robust blood vessel growth to support skin restoration (Fig. 1H). As an example, *Hif1a* and *Arnt* exhibited a significant increase in expanded epidermal, dermal, and immune cell clusters (Fig. 1H, I). The spatial density heatmap of key transcripts showed a higher enrichment of angiogenesis genes in the expanded skin (Fig. 1J). The angiogenesis genes are distributed across the entire skin, with higher expression in the epidermis compared to the dermis (Fig. 1J).

Furthermore, stress granule related score is significantly elevated across epidermal and dermal cell types (Fig. 1H). Genes associated with stress granules that modulate stress responses[28], such as *G3bp1 and Pabpc1*, were elevated across the skin cell groups (Fig. 1I, bottom).

https://doi.org/10.1038/s41467-025-62270-3

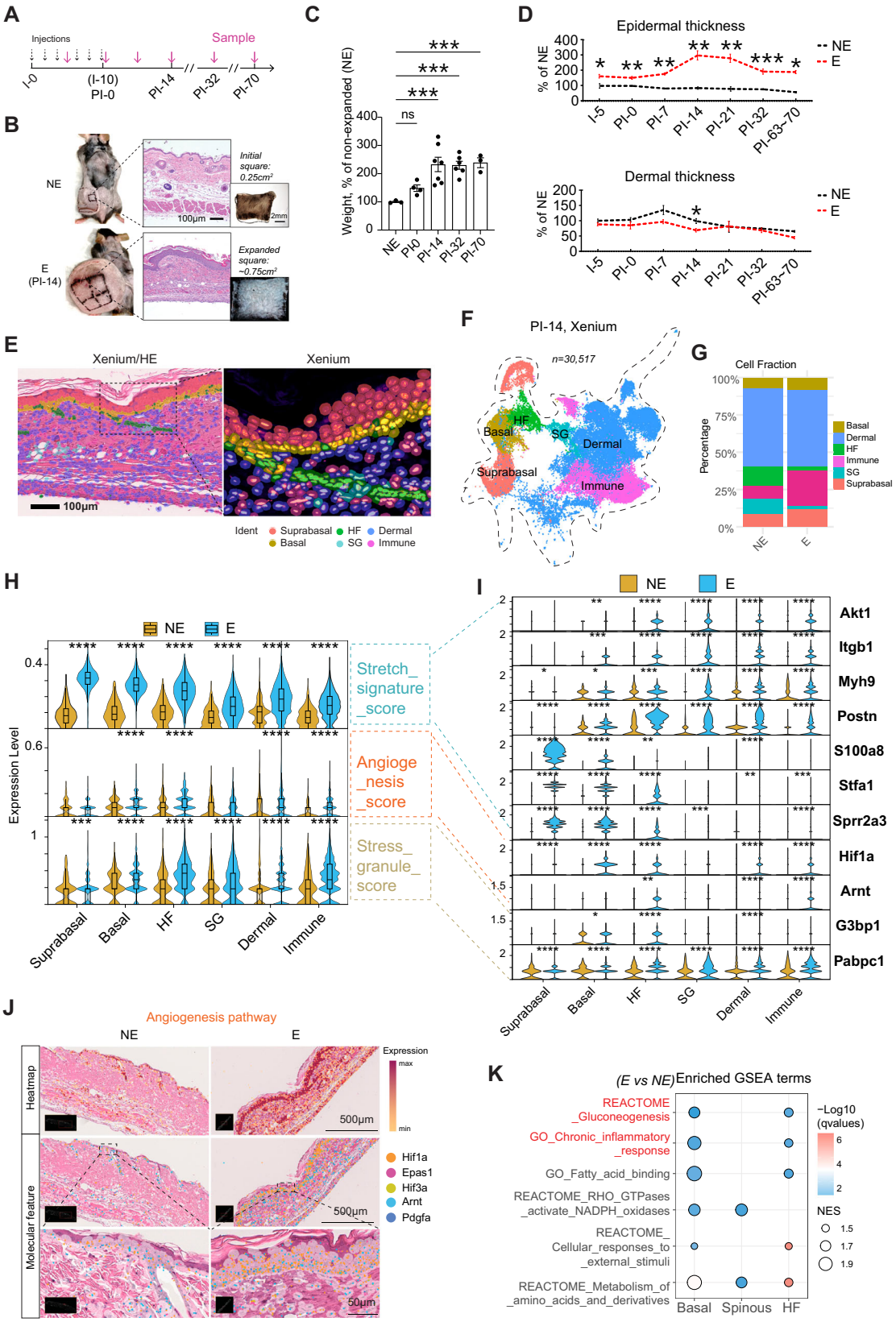

Tension activates an inflammatory-metabolic molecular network

To molecularly define the events occurring during epidermal thickening, we isolated epithelial cells for single-cell sequencing to observe biological changes in identified cell clusters (Figs. S2A, S2B). By examining the expression of known cell type-specific markers, we categorized 13 clusters (Fig. S2B) falling into four major cell types (Fig. S1A), including spinous cells (Krt1$^+$ and Krt10$^+$), basal cells (Krt14$^+$ and Krt5$^+$), proliferating basal cells (Mki67$^+$, Krt14$^+$, and Krt5$^+$), HF-associated cells (Krt15$^+$, Krt17$^+$, and Krt79$^+$), Hair follicle stem cells (HFSCs, Lgr5$^+$ and Cd34$^+$), sebaceous glands (SG, Mgst1$^+$ and Scd1$^+$), and immune cells (Cd3g$^+$, Cd207$^+$). Gene set enrichment analysis

Fig. 1 | Tension activates an inflammatory-metabolic molecular network in the skin. A tissue expansion (TE) protocol. I-#, injection day #; PI-#, post-last injection day #. **B** Representative images of pre- and post-TE, along with skin histology. **C** Skin weight changes post-expansion. (n = 3–7). **D** Quantification of skin layer thickness. (n = 3–8). **E** Spatial clustering of expanded skin with post-xenium HE. NE has one piece of tissue; E has 2 pieces of tissue. **F** Integrated UMAP of cell clusters from Xenium assay. Cells include both NE and E samples. **G** Identified cell type fractions from Xenium assay. **H** Pathway scores from Xenium assay. **I** Representative Genes' expression of different pathways among different cellular populations. **J** Upper: spatial heatmap of angiogenesis pathway; middle: spatial plot of angiogenesis genes in skin; lower: high-resolution spatial map of angiogenesis genes in NE and E skin. **K** Gene Set Enrichment Analysis (GSEA) of scRNA-seq, grouped by cell type. To perform univariate statistical analysis, the two-sided Student's t-test was used. For multivariate analyses, the one-way ANOVA test was used. The Wilcoxon rank-sum test was used for all violin plots in this manuscript. Abbreviations: E the skin overlying the inflated expander, NE the skin overlying the expander in mice where the expander was not inflated. NES normalized enrichment score, HF hair follicle, SG sebaceous gland.

(GSEA) confirmed that expanded basal and HF cells undergo a significant cellular response to external stimuli (Fig. 1K). Confirming our spatial transcriptomics, the cells from expanded skin are enriched in pathways relating to cellular response to external stimuli, inflammatory response, glucose metabolism, and other metabolic-related pathways (Fig. 1K).

Tension induces an inflammatory signature in expanded skin

To better understand the inflammatory changes resulting from tissue expansion, we performed gene set enrichment analysis (GSEA) using all epidermal cells from single-cell RNA sequencing (scRNA-seq) data. The study revealed that stretched keratinocytes exhibit enrichment in several inflammation-related pathways, such as chronic inflammatory response, leukocyte migration, and production of molecular-mediated inflammatory response (Fig. S2C, D). These findings suggest that stretched keratinocytes release signals that attract immune cell infiltration and enhance inflammation as a primary response to tissue expansion.

We then investigated how stretching affects the communication between different cell types. Using CellChat[29], we inferred the cell-cell communication of epidermal cells and observed distinct patterns and strengths of interactions between NE and E epidermal cells (Fig. S2E). Specifically, hair follicle stem cells (HFSC) had reduced activity after stretching, consistent with our previous stem cell lineage-tracing results[30]. Expanded cells showed increased activity in sending and receiving inflammatory signals (Fig. S2F), including the CXCL, CCL, TNF, and TGF-β signaling.

Furthermore, we calculated the communication probability of inflammatory-related pathways and found differential crosstalk of CXCL, CCL, TNF, and TGF-β signaling in the stretched epidermal cells (Fig. 2A). Upon stretching, keratinocytes sent more CXCL signaling and received more TNF signaling from immune cells (Fig. 2A). Additionally, TGF-β signaling was enhanced, particularly in the upper (infundibulum, HF I) and middle (HF II, III) hair follicle cells (Fig. 2A). Specifically, we see more basal-immune cell interactions of CXCL signaling after expansion (Fig. 2A). These analyses support a keratinocyte-induced metabolic inflammation after tissue expansion.

Next, we used xenium to confirm and map the inflammatory cytokines in the skin. By creating a spatial plot overlaid with post-xenium HE, we visualized the distribution of a selected list of cytokines in both non-expanded (NE) and expanded (E) skin samples. In general, stretched skin expressed more cytokine transcripts (Fig. 2B). Statistically, we identified significantly higher Immune pathway scores in E samples, depending on the expressions of these cytokines (Fig. 2C, upper panel). The immune_score shows significant elevation in both the epidermal and dermal cells in the expanded (E) skin (Fig. 2C). These findings confirm that tissue expansion activates an inflammatory signature in the skin.

Tension induces immune cell infiltration in the skin

We then experimentally confirmed the changes in the immune cells in response to stretching. We started by defining the types of immune cells present in the skin of mice in the tissue expansion model. We collected fresh skin samples from mice with and without tissue expansion 14 days after the initial procedure and used flow cytometry to analyze the changes in immune cells (Fig. S3A). We found that tension induces significant immune cell infiltration into the skin, predominantly myeloid cells but not lymphoid T cells (Fig. 2D, E, Fig. S3A). In particular, mostly macrophages but also neutrophils and monocytes infiltrated into the stretched skin (Fig. 2D, E). Consistent with these findings, we observed a significant general infiltration of immune cells ($CD45^+$) in the expanded skin, suggesting a sterile and prolonged inflammation due to stretching (Fig. 2F, G, Fig. S3B). However, tension reduced the amount of epidermal Langerhans cells (LC) with mild but insignificant increases in dermal dendritic cells (DC) (Fig. 2F, G). Immunofluorescence analysis confirmed the increased presence of $CD68^+$ macrophages in the stretched skin (Fig. 2H).

Skin expansion alters the circulating blood cell profile

We next examined whether tension-induced inflammatory changes were confined to the skin or manifested systemically as well. After performing tissue expansion, we collected blood cells from both non-expanded (NE) and expanded (E) mice 14 days post-injection, and then isolated peripheral blood mononuclear cells (PBMC) for RNA-sequencing (Fig. S4A). We found 1037 differentially expressed genes (DEGs), including 767 upregulated and 370 downregulated genes (Fig. S4B). The GO analysis revealed higher activation of myeloid lineages and lower activity of lymphoid lineages of immune cells in E-PBMC (Fig. S4C–F, pathways marked with red *). Additionally, E-PBMC showed upregulated pathways related to Hif-1 signaling and glycolysis/gluconeogenesis, which is consistent with our findings from single-cell sequencing (Fig. S4E, pathways marked with blue *). Interestingly, we observed downregulation of pathways associated with insulin secretion and type I diabetes, implying systemic metabolic changes resulting from local skin expansion (Fig. S4F, pathways marked with green *). Though PBMCs do not secrete insulin, these pathway changes reflect an overlap to PBMC responses that indicate metabolic and inflammatory states and suggest systemic metabolic changes that are relevant to these pathways or an involvement of the immune system in these biological processes.

We next collected circulating PBMCs from NE and E mice, and checked their myeloid lineage cell fraction changes, and found $CD11b^+$ myeloid cells have decreased circulating proportion in E (expanded) mice vs NE (nonexpanded) controls. Given our discovery of increased myeloid cells in the stretched skin, these results indicate a robust mobilization of myeloid cells from the blood to skin after TE, diminishing the circulating population (Fig. S3C). In all, coincident with tissue expansion induced skin growth is mobilization of circulating Myeloid cell populations into the skin, consistent with the known contribution of myeloid cells for tissue restoration in multiple contexts. These results demonstrate non-local effects on organismal physiology after skin expansion.

Tension increases glucose metabolism in the skin

In our scRNA-seq analysis of stretched keratinocytes, we observed changes in the glucose metabolic pathway (see Fig. 3A). Interestingly,

https://doi.org/10.1038/s41467-025-62270-3

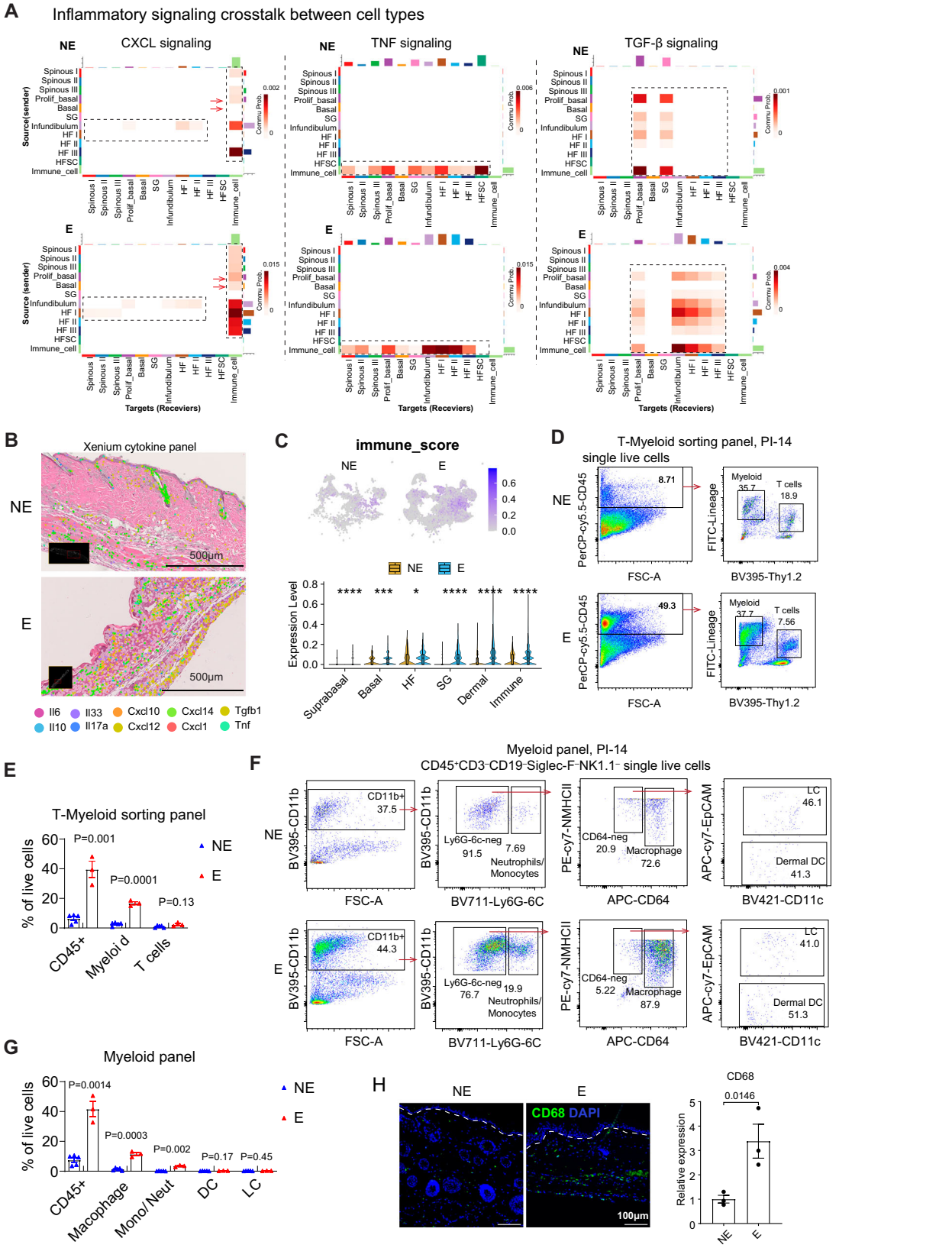

we found that glucose metabolism and the glycolysis pathway are enriched in stretched keratinocytes. In contrast, the insulin-mediated glucose uptake pathway is decreased (see Fig. 3A). Instead, the non-insulin-dependent glucose transporter Glut1 was elevated (Slc2a1). Slc2a1 (*Glut1*) is one of the most upregulated genes after tissue expansion in the epidermal scRNA-seq data (Fig. S5A, Fig. 3B). Other glycolysis-related genes, such as *Pgk1*, *Pkm*, and *Ldha* are upregulated in both datasets, while *Aldoa* is upregulated in epidermal scRNA-seq but downregulated in the skin microarray (Fig. S5A, Fig. 3B).

To investigate changes in glucose metabolism throughout the skin, we reexamined our xenium assays and evaluated the expression of genes related to glycolysis in the skin (Fig. 3C). The spatial plot

Fig. 2 | Mechanical tension induces immune cell infiltration in the skin. A The heatmap quantification of signaling communication probability across distinct cell types. Boxes mark the differential crosstalk between cells. Arrows on the left panel show basal-immune interactions. **B** Spatial plot of selected cytokines from xenium assay. **C** The upper UMAP shows immune_score based on the expression of the cytokine panel list in (**B**). The below violin plot showed immune_scores across various cell types between E and NE. **D**, **E** Flow cytometry for T-Myeloid sorting among isolated single cells from skin samples of PI-14. Cells in the left square are selected as single live cells. Immune cells are gated as $CD45^+$. The FITC lineage antibody is a cocktail of FITC anti-mCD3ε/FITC anti-mGr-1/FITC anti-mCD11b/FITC anti-mCD45R(B220)/FITC anti-mTer-119. The lineage antibody mix reacts with major hematopoietic cell lineages, such as T lymphocytes, B lymphocytes, monocytes/macrophages, granulocytes, NK cells, and erythrocytes. The Lin^+ $Thy1^-$ cells are myeloid cells. The majority of Lin^+ $Thy1^+$ cells are T cells. NE, n = 5, E, n = 3. **F**, **G** Flow cytometry analysis of Myeloid cells. Gate for $CD45^+$ $lineage^-$ ($Siglec\text{-}F^-$, $CD3e^-$, $CD19^-$, and $NK1.1^-$) to exclude eosinophils, T cells, B cells, and NK cells. $Lineage^-$ $CD11b^+$ Ly6G/6 C^+ cells are identified as monocytes/neutrophils (Ly6G/$6C^+$) and macrophages ($CD64^+$). From the $CD11b^+$ $Ly6c^-$gate, macrophages ($EpCAM^-CD64^+$), Langerhans cells (LC, $CD64^-EpCAM^+$ MHC II^+), and dermal dendritic cells (DC, $CD64^-EpCAM^-$MHC II^+CD11c^+) are identified. (n = 3). **H** $CD68^+$ macrophages accumulate in expanded skin samples as measured by immunofluorescence. Dashed lines were used to separate the epidermis and dermis. (n = 3). To perform univariate statistical analysis, the two-sided Student's t-test was used. For multivariate analyses, the one-way ANOVA test was used. Wilcoxon rank-sum test was used for all violin plot in this manuscript.

revealed an overall enrichment of glycolysis genes in the E skin. quantification of Glycolysis_score is elevated in E skin, with significant increase in all cell types (Fig. 3D, left). Genes such as *Glut1 (Slc2a1), Aldoa, Pkm*, and *Pgk1* showed increased expression in the epidermal cell clusters, consistent with single-cell sequencing (Fig. 3D, right panel). Furthermore, dermal cells and immune cells also exhibited significantly increased expression of glycolysis genes, including *Pgk1*, *Pkm*, *Aldoa*, *Glut1*, and *Ldha*, indicating that tension induces an overall alteration in glucose metabolism across the skin tissue (Fig. 3D). Immunofluorescence staining confirmed elevated levels of the glycolysis genes *Glut1* and *Aldoa* in expanded skin (Fig. 3E). Interestingly, Glut1 was expressed in the basal stem cells, while Aldoa was more prevalent in suprabasal cells (Fig. 3E). Altogether, these results demonstrate tissue wide increases in glycolysis to satisfy the energy demands of organ size increase.

Skin TE has no short-term impact on systemic glucose metabolism

Our results indicate that stretched skin modifies glucose metabolism and inflammation locally and systemically (Figs. 1–3 and S2–4). This mimics the chronic inflammation and metabolic disorders such as type 2 diabetes that are associated with obesity[31]. Our initial data indicate that skin TE does not affect blood glucose levels in mice at PI-14 (Fig. S6A). Nevertheless, given the overlapping features in both obesity and our TE model of stretching, skin growth, inflammation, and dysmetabolism, we tested whether skin stretching in the absence of obesity in our model contributes to systemic glucose metabolism dysregulation and insulin resistance. To test this, we measured changes in systemic glucose metabolism in the mice using the Insulin Tolerance Test (ITT) and Glucose Tolerance Test (GTT) assays[32]. We prepared mice with and without skin stretching on PI-14 and performed ITT and GTT assays separately (Fig. S6B). We fasted mice for 5 h before the insulin or glucose challenge (Fig. S6C). We examined the changes in raw blood glucose numbers (Fig. S6D, E, left panels) and normalized them to baseline (Fig. S6D, E, right panels). The mice with skin stretching had lower blood glucose levels, and we see skin stretching slightly improved glucose tolerance and insulin sensitivity through no significant ITT and GTT differences were observed by using the area under curve test (Fig. S6D, E). Thus at least in the conditions tested here, acute local skin stretch did not change body-wide glucose catabolism and needs further testing in the context of chronic changes.

Epidermal-Piezo1 knockout impairs skin expansion

Given these local effects, we hypothesize that skin mechanosensing induces tissue growth and is accompanied by elevated local inflammation and metabolic reprogramming. We next sought to define the mechanosensors that mediate these changes (Fig. 3F). Piezo1 has been reported to be separately associated with both modified metabolism and inflammation[33,34], which matches our findings from the TE model. It is a calcium-permeable cation channel abundant in mechano-active tissues such as epidermal keratinocytes[24]. Notably, our single-cell sequencing identified the top two upregulated genes, S100A8 and S100A9, both of which are associated with calcium signaling pathways. Piezo1 regulates wound repairing, modulates cutaneous mechanosensation[24], and connects mechanosensing with inflammation in the skin. In a model of mechanical force-induced stress in the skin, researchers demonstrated that knocking down Piezo1 in epidermal stem cells reduces the immune activation pathways[35]. Thus, we hypothesize that Piezo1, a mechanically gated calcium-permeable cation channel[24], acts as the mechano-transducer in stretched keratinocytes to mediate the downstream response. To test this hypothesis, we established a mouse strain to conditionally delete epidermal Piezo1 upon TAM injection (Fig. 4A, B). TAM injections significantly knocked down Piezo1 gene expression in this K5;P1f mouse line (Fig. 4C).

We examined the effects of epidermal Piezo1 deletion on skin growth during tissue expansion (Fig. 4D). We found that surface area growth was markedly attenuated in the tissue expanded K5;P1f animals (Fig. 4E, F). The skin weight is decreased in K5;P1f animals ($P = 0.10$), with significant reduction of epidermal and dermal thickness (Fig. 4G, H, I). We then investigated how epidermal Piezo1 affects tension-induced inflammatory-metabolic network changes. Immunofluorescence staining showed that after Piezo1 deletion, the expanded mice exhibited decreased macrophage infiltration, accompanied by lower expression levels of the glycolysis proteins Glut1 and Aldoa (Fig. 4J, K). Glut1, which is prevalent in basal stem cells, was significantly reduced in K5;P1f animals after expansion (Fig. 4J, K). In summary, epidermal Piezo1 deletion impairs skin growth and molecular network changes during TE.

Piezo1 activator promotes tissue expansion

Given that loss of function in Piezo1 inhibited tissue expansion, we next sought to test if gain of function of Piezo1 could augment tissue expansion. We tested whether chemically activating Piezo1 could enhance our in vivo tissue expansion (TE) model. We applied Yoda1, a small molecule Piezo1 agonist[36] (Fig. 5A). Yoda1-treated animals exhibited a more rapid increase in skin surface area and achieved a larger final size compared to the untreated control E group (Fig. 5A, B). The Yoda1-treated animals also showed increased skin weight (Fig. 5C), with a significantly thicker epidermal layer and a thinner dermal layer (Fig. 5D, E).

To test for the augmentation of other skin stretch features after Piezo1 activation, we collected samples treated with Yoda1 along with untreated samples at the PI-7 time point for the spatial transcriptomics (Xenium) assay. The spatial plot revealed six main clusters of cells identified from Xenium (Figs. S7A, B and 5F), which were spatially distributed in the same pattern as post-Xenium HE (Fig. 5F). Cell fraction analysis indicated that Yoda1 treatment further increased the

https://doi.org/10.1038/s41467-025-62270-3

basal and suprabasal cell fractions after expansion while decreasing the sebaceous gland (SG) and hair follicle (HF) cell proportions (Fig. 5G). Separated cluster mapping further shows decreased SG and HF in Yoda1-treated group (Fig. 5H).

We examined the previously studies pathways (as presented in Fig. 1H), which are increased in the E group compared to the NE control (Figs. 1H, 5I). After Yoda1 treatment, we observed a further increase of these pathways in the suprabasal, basal, HF, dermal, and immune cells when compared to the untreated E group, including Stretch_signature_score, Angiogenesis_score, and Stress_granule_score (Fig. 5I, left). We further investigated the expression of representative genes within these pathways (Fig. 5I, right). For example, *Akt1*, which mediate skin

Fig. 3 | Tension enhances the glycolysis pathway in the skin. A Glucose metabolic-related pathway enrichment analyses of stretched keratinocytes versus controls. Pathways with a positive score are increased after stretch. **B** Heatmap of glycolysis pathway-related gene expression levels. **C** upper: spatial heatmap of glycolysis pathway; middle: spatial plot of glycolysis-related genes; lower: high-resolution spatial map of glycolysis genes in NE and E skin. **D** The upper UMAP shows Glycolysis_score based on the expression of the gene panel list in (**C**). The left below violin plot shows Glycolysis_scores across various cell types between E and NE. The right violin plot shows the expression of the representative glycolysis genes in xenium clusters. **E** Immunofluorescence of glycolysis-related genes Glut1/Slc2a1 and Aldoa in the E and NE samples of the epidermis. Followed by expression level quantification. (n = 3). **F** Running summary. To perform univariate statistical analysis, the two-sided Student's t-test was used. For multivariate analyses, the one-way ANOVA test was used. The Wilcoxon rank-sum test was used for all violin plots in this manuscript.

growth and tissue repair, is significantly increased in E-Yd1 versus E-con samples (Fig. 5I). Other genes including *Itgb1* and *Myh9*, which sense mechanical stress in the skin niche[11,20], *Postn*, which is linked to mechanical sensing and restoration[27], are all significantly amplified across different cell types in E-Yoda1 group compared to E-con samples (Fig. 5I, right). Some genes exhibited differences between epidermal and dermal cells. For instance, *S100a8*, *Stfa1*, and *Sprr2a3* were significantly elevated in epidermal cells with robust expression, and are boosted by Yoda1-treatment, but not in dermal and immune cells (Fig. 5I, right). Stress granule-related genes *G3bp1* and *G3bp2*, show enhanced expression in the E-Yd1 group (Fig. S7C). Specifically, *G3bp1* is higher in basal, HF, and SG cell clusters, and *G3bp2* is higher in HF groups (Fig. S7D). These findings suggest that Yoda1-induced activation of Piezo1 in the skin amplifies tension-induced biological changes and gene signatures.

The spatial heatmap also showed enhanced enrichment of angiogenesis-related genes in the Yoda1-treated group (Fig. 5J, upper panel), distributed across the entire skin (Fig. 5J, lower panel). A violin plot showed increased *Hif1a* in all cell types of the Yoda1-treated expanded skin compared to the untreated (E-con) and NE controls (Fig. 5I).

The growth-related gene Akt was found to be increased in the groups treated with Yoda1, as compared to the non-treated E group (Fig. 5I). Tension-induced skin growth is based on cell hyperproliferation and is dependent on the Hippo effector YAP[11]. We evaluated the proliferation marker Ki67 and Yap1 changes, which have previously been confirmed to be induced by tension[11]. Yoda1 treatment does not significantly induce transcripts of these genes. However, immunofluorescence reveals significantly higher $Ki67^+$ cell numbers after Yoda1 treatment (Fig. 5K, L). Additionally, the number of nuclear YAP^+ cells is significantly increased, particularly in the basal layer of progenitor keratinocytes, indicating more active expansion (Fig. 5K, L).

In summary, the in vivo activation of Piezo1 with Yoda1 induces greater YAP nuclear translocation in epidermal stem cells to accelerate tissue expansion (Fig. 5M).

Piezo1 activation amplifies metabolic and inflammatory changes

Tension in the skin leads to changes in the inflammatory and metabolic networks underlying skin growth (Fig. 1G, K, Fig. 2, and Fig. 3). We wanted to find out if activating Piezo1 accelerates these network changes. We mapped the cytokine and glycolysis genes in our spatial transcriptomics data (Fig. 6A, B). A spatial heatmap revealed that skin treated with Yoda1 showed a higher cytokine panel score and greater expression of related genes, evident in all skin layers (Fig. 6A). In another spatial heatmap, the glycolysis gene panel scored more highly in the Yoda1-treated expanded group compared to the untreated expanded group and was distributed throughout the skin (Fig. 6B).

We tested if inflammation and glycolysis pathway score changes after skin stretch could be accelerated with Piezo1 activation. We found that Yoda1 treatment elevated immune_score across all cell types (Fig. 6C). Similarly, the Glycolysis_score is also boosted by Piezo1 activation through Yoda1 treatment and are significant across all cell types (Fig. 6D, left). Furthermore, gene expression analysis showed that activating Piezo1 with Yoda1 led to an increase in tension-induced glycolysis transcripts in multiple cell clusters, including *Glut1*, *Aldoa* and *Ldha* (Fig. 6D, right).

We also investigated the modification of other metabolic pathways. We found that the fatty acid binding pathway is another enriched metabolic term in stretched cells (see Fig. 1K, S8A). Further analysis using a heatmap revealed an increase in the expression of genes related to the fatty acid binding pathway in stretched epidermal cells, with Fabp5 being among the top 3 genes (see Fig. S8B). When subjected to tension, Fabp5 expression increased in various cell types, including basal, HF, and spinous cells, as well as dermal and immune cells (see Fig. S8C, D). Additionally, we found that Yoda1-induced activation of Piezo1 further elevated Fabp5 expression across the entire skin (see Fig. S8D).

To verify these findings, we did immunofluorescence staining and observed significantly increased infiltration of $CD68^+$ macrophages and elevated expression of glucose metabolism proteins Glut1 and Aldoa in the Yoda1-treated group (Fig. 6F, G). These findings demonstrate that activating Piezo1 with Yoda1 accelerates the main molecular features seen in skin stretch—increased immune infiltration and the glycolysis pathway.

Discussion

Tissue expansion, a process in which the skin is stretched to stimulate growth, provides a unique opportunity to study the adaptive responses by which physical forces lead to organ growth. Our findings here provide crucial insights into the mechanobiology of skin restoration, particularly in the context of clinical tissue expansion (TE). The identification of an enhanced immuno-metabolic network in stretched skin, as revealed through single-cell and spatial transcriptomics, sheds light on the cellular and molecular changes underlying tension-induced growth dynamics in skin. We find that the mechanotransducer Piezo1 is a key upstream regulatory orchestrating these responses and enabling skin growth.

Heterogeneous response of skin compartments to mechanical tension

Skin exhibits nonhomogeneous mechanical stability; different constituent cell types modulate or react to stretch differently. For example, from our previous work, we found the hypodermis layer decreases following TE, while the epidermal layer exhibits robust growth, and the dermal layer shows no significant depth change. More specifically, we found that while epidermis displays robust growth during tissue expansion, with significant contributions from $Lgr6^+$ epidermal stem cells through the Hippo pathway activator YAP[11], dermal expansion is much more modest. The mechanisms responsible for the disparate effects of tension in skin elements are unknown and of biologic and clinical importance. Poor expansion of the dermis leads to erosion and expander exposure during tissue expansion and underlies pathologic striae observed in pregnancy and obesity. However, in a recent study, inhibiting YAP in dermal fibroblasts reduces the fibrotic response and promotes wound regeneration[37], indicating that the differing responses of the epidermis and dermis during tissue expansion may arise from their varied reactions to the same signals. In another study, converting fibroblasts toward a pro-regenerative, adipogenic state similar to unwounded skin during autologous split-thickness skin grafting (STSG)[38] inhibited scarring, suggesting that modulating fibrosis may facilitate dermal restoration during tissue expansion.

https://doi.org/10.1038/s41467-025-62270-3

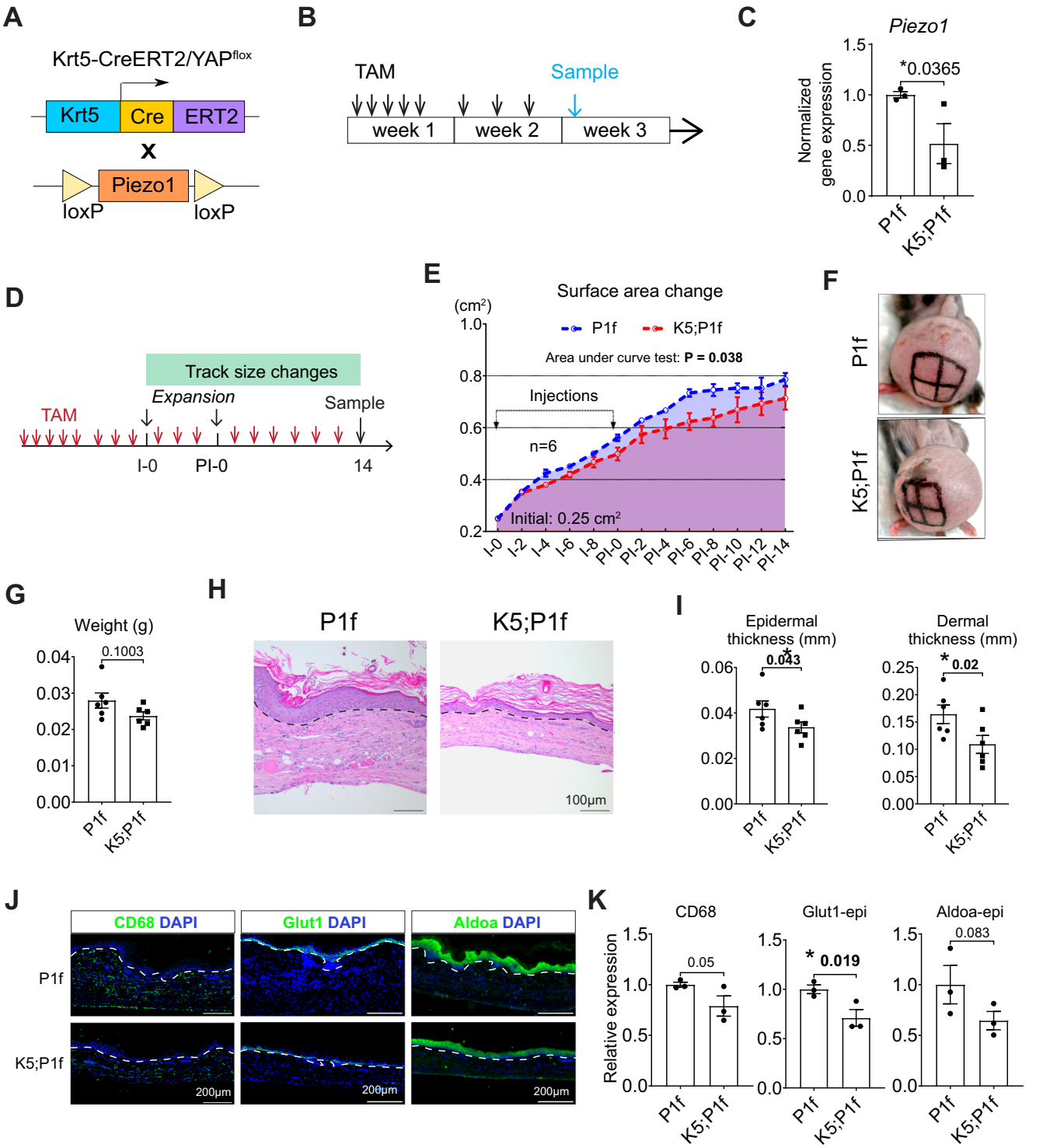

Fig. 4 | Loss of Epidermal-Piezo1 inhibits tissue expansion in vivo. A Breeding strategy to delete Piezo1 in Krt5^{+} skin stem cells using Cre-Loxp recombination. **B** workflow of tamoxifen injections for K5-cre;Piezo1-flox (K5;P1f) mice to induce gene knockout. **C** RT-PCR reveals Piezo1 knockout efficiency in K5;P1f strain compared to P1f control strain. (n = 3). **D** Tissue expansion workflow in K5;P1f strain and control strain. **E** Surface area quantification shows that Piezo1 knockout in the epidermis significantly decreases stretch-induced skin growth. The area under curve comparison was used. **F** Representative image of expanded P1f and K5;P1f mice at PI-14. **G** Skin weight changes. (n = 6). **H, I** Epidermal-Piezo1 knockout decreases stretch-induced skin weight and epidermal thickness after skin stretch. (n = 6). **J, K** Immunofluorescence staining of macrophage marker CD68, and glycolysis markers Glut1 and Aldoa, followed by quantification. CD68 is quantified in the dermis, and Glut1 and Aldoa are quantified in the epidermis. (n = 3). To perform univariate statistical analysis, the two-sided Student's t-test was used. For multivariate analyses, the one-way ANOVA test was used.

https://doi.org/10.1038/s41467-025-62270-3

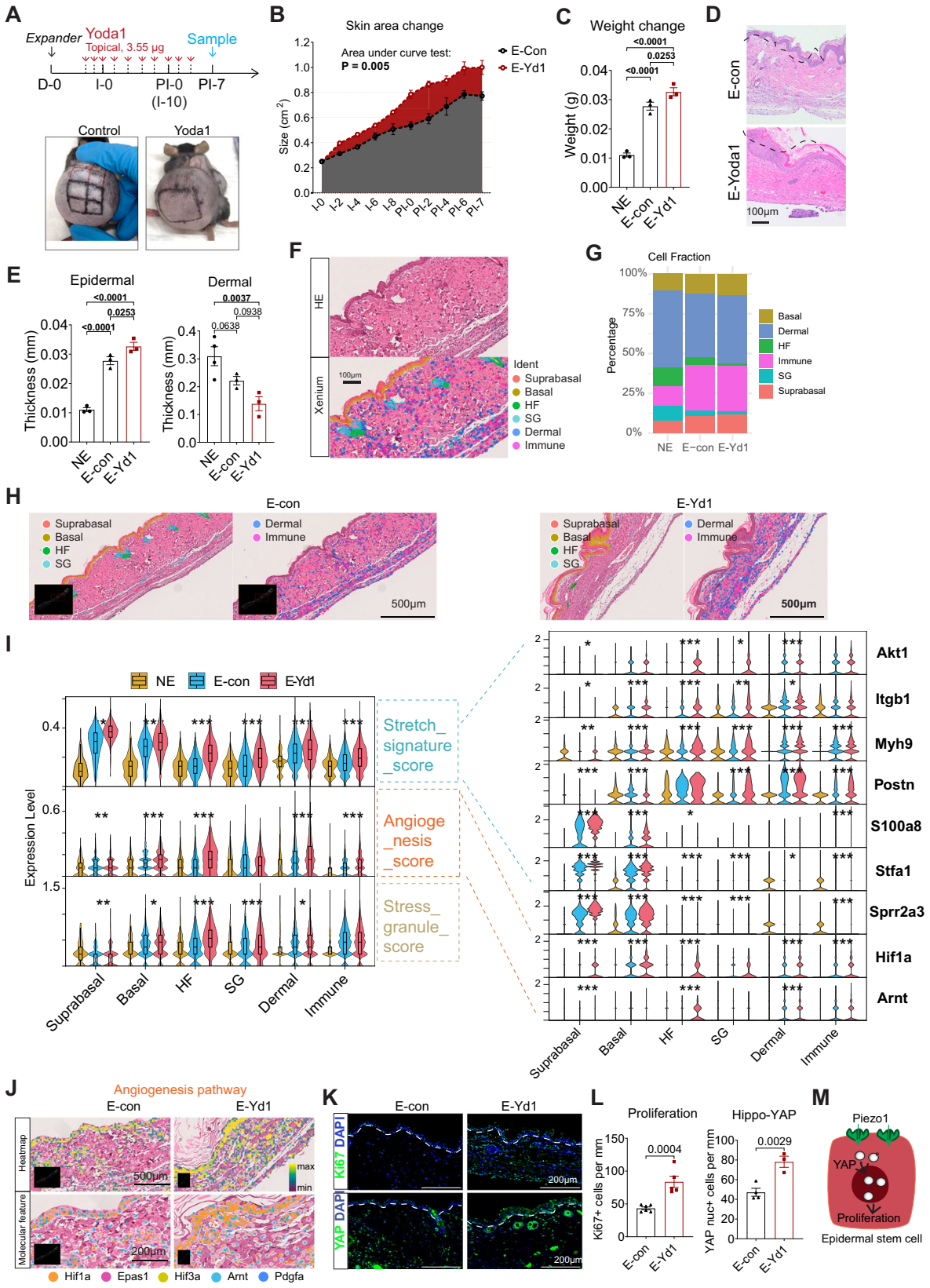

A related question to the heterogeneous responses of different skin compartments to stress is whether one functionally might induce the other. For example, could the notable decrease in hypodermal adipocytes induce the hyperproliferation of the epidermis? Future studies should dissect these possibilities. One argument against the loss of adipocytes inducing stretch-induced epidermal thickening is that adipocyte-related factors, such as Leptin, IGF1, and adiponectin, are most commonly associated with keratinocyte growth[39–41]. In this context, the loss of the adipocytes as seen in the TE model might be predicted to lead to less keratinocyte proliferation, not more keratinocyte proliferation as seen in our TE model.

Fig. 5 | Piezo1 activation promotes tissue expansion in vivo. A Timeline of Piezo1 activator Yoda1 topical application during tissue expansion in mice, with representative images of expanded skin on PI-7. **B**–**E** Increase in skin surface area, weight, and epidermal thickness, and decreased dermal thickness in Yoda1-treated mice during tissue expansion. (n = 3). **F** Spatial clustering of expanded skin with post-xenium HE. NE has one piece of tissue, E-con has two pieces of tissue, and E-Yd1 has two pieces of tissue. **G** Identified cell type fractions from Xenium assay. **H** Mapping Xenium cell cluster location with HE staining. **I** Left: Pathway scores from Xenium assay. Right: Representative Genes' expression of different pathways among different cellular populations. Significant test results between E-con and E-Yd1 samples were labeled on the violin plot. Detailed comparison results can be found in supplementary datasets. **J** upper: spatial heatmap of angiogenesis pathway; lower: spatial plot of angiogenesis-related genes. **K**, **L** Immunofluorescence staining of proliferation marker Ki67 and Hippo pathway effector YAP protein, followed by quantification. Ki67 and YAP are quantified in the epidermis. (n = 3). **M** Running summary. Abbreviations—E-con: expanded mice, serve as a control for Yoda1-treated mice. E-Yd1: expanded mice with Yoda1 treatment. For multivariate analyses, the one-way ANOVA test was used. For two-group comparisons, the two-sided Student's t-test was used. Wilcoxon rank-sum test was used for all violin plots in this manuscript.

Tissue expansion: contrast between tension in the tissue expansion model and wounding

Mechanical stress has been associated with fibrosis and scar formation during wounding and skin repair, which contrasts with the regenerative skin expansion during TE. Indeed, previous research has demonstrated that mechanical tension on the skin is a critical trigger of keloid generation after wounding, particularly in individuals who are genetically predisposed to develop keloids[42]. Furthermore, mechanical strain-induced myeloid cell recruitment and differentiation in the skin could drive such fibrotic processes[43]. In further support of the deleterious effects of tension, pharmacological blockade of mechanotransduction with small-molecule focal adhesion (FAK) inhibitor significantly improves large animal skin healing[44]. Also, the relief of mechanical stress at the diabetic wound edges using a strain-programmed patch promotes faster re-epithelialization with enhanced angiogenesis and enriched pro-regenerative fibroblast populations[45]. This evidence might suggest that in our TE model, tension would only have negative effects on fibrosis.

However, the role of mechanical tension in our TE is a distinct context from the wounding in the skin. The model of tissue expansion lacks the abrupt injury and trauma to create a localized lesion seen in wounding. Instead, the expander-induced tension promotes skin growth while and growth inducing time-dependent extensive molecular changes[38] over a cohesive large area. These changes include mechanoresponsive genes that relate to immune response, cell metabolism switches, muscle contraction and cytoskeleton organization. Thus, the effects of tension are likely context-specific and not uniquely related to scarring.

Role of myeloid innate immune cells in mechanosensation

The skin cell senses mechanical cues and converts them into biochemical signals during tissue expansion (TE). We observed a highly modified communication of biological signals within the expanded skin cells (Fig. S2E), which suggests a change in the tissue microenvironment due to mechanotransduction. Additionally, there is heightened inflammatory crosstalk in stem cells and immune cells, but not in the differentiated spinous cells (Fig. 2A). The expanded skin tissue also shows an elevated local inflammatory response, leading to an increased influx of myeloid innate immune cells to the skin (Fig. 2D–F). We also found that the blood cell profiles shift towards more myeloid activation, as circulating myeloid cells are mobilized to skin with resultant increases in skin macrophages, underscoring the overall impact of local skin expansion on body-wide physiology. The mechanisms underlying the change in immune profile and its consequences for skin growth are important areas for investigation.

Mechanical forces clearly play a crucial role in activating and influencing immune cells. The stiffness of the extracellular matrix (ECM) affects immune cell behavior[46,47]. For example, the ECM integrin receptors are also mechanotransducers[48]. In our study, the ECM proteins ITGB1 and TNC were significantly increased in expanded skin. These proteins maintain cell stemness and are linked to immune cell infiltration in chronic inflammation[48] and cancer[49], suggesting that ECM changes in parallel modulate stemness and immune cell accumulation in expanded skin.

Mechanotransduction in cells often has a significant impact on immune cell recruitment[46,47]. For instance, fibroblasts can detect ECM mechanics and, as a result, recruit immune cells like macrophages[50]. In the expansion group, epidermal cells released more CXCL signaling compared to the control group. We cross-referenced spatial transcriptomics to single-cell RNA sequencing to map the cytokines in highly interconnected pathways. The cytokines *Cxcl12* and *Cxcl14* most significantly increased in expanded skin tissue, particularly among epidermal and dermal non-immune cells (see Fig. 2B). CXCLs can act as chemoattractant for immune cells, potentially contributing to the infiltration of immune cells in the expansion model.

The heightened immune response in TE is indicative of the intricate interplay between mechanical stimuli and immune cell dynamics in the skin growth process. However, the functional consequences of tension-induced inflammation require further investigation. In a prior study, tissue-resident macrophages were key contributors to skin growth tissue-resident macrophages in skin growth during tissue expansion, indicating that managing inflammation could be a key strategy for promoting skin growth under mechanical strain[21]. However, broad inhibition of adaptive immunity in skin with corticosteroids did not affect tissue growth during TE[20]. Considering our transcriptomics, immunofluorescence, and flow cytometry, we conclude that myeloid cells have a more significant presence in TE than lymphoid cells.

To summarize, tissue expansion coincides with the mobilization of circulating myeloid cell populations to infiltrate into the skin. This supports the well-established literature on the support of myeloid and specifically macrophage populations to tissue restoration in multiple contexts[6]. However, further investigation is needed on the particular biological role of myeloid mobilization into the skin in the tissue expansion model.

Glucose metabolism rewiring

Significantly increased glycolysis pathway scores were noted in the expanded skin at both PI-7 and PI-14 time points, indicating the importance of metabolic adaptations for tissue growth. The *Aldoa*, *Pkm*, and *Ldha* genes showed increased expression across all cell types, while *Glut1* and *Pdk1* genes exhibited changes primarily in the epidermal clusters (Fig. 3D; Fig. 6E, bottom). The level of *Ldha* is significantly increased in expanded cell clusters, indicating an induction of anaerobic glycolysis after tissue expansion. Immunofluorescence staining confirmed tension-induced levels and location of Glut1 and Aldoa proteins. Treatment with Yoda1 amplified all these induced changes and further promoted tissue growth, indicating the crucial role of Piezo1 in tension-induced skin growth and metabolic changes.

Glut1 serves as the primary glucose transporter in the epidermis, playing a crucial role in glucose uptake and regulating keratinocyte growth[51,52]. Given its involvement in controlling keratinocyte proliferation and immune regulation, Glut1 is a potential factor in the management of inflammatory skin diseases[51,52]. Glut1 is a downstream target of Piezo1 activation and has higher expression in the epidermis than in the dermis (Figs. 3D, 6E). Removing Glut1 from the epidermis hinders keratinocyte proliferation following damage[51], making it a promising target for promoting tissue growth. Further investigation is

https://doi.org/10.1038/s41467-025-62270-3

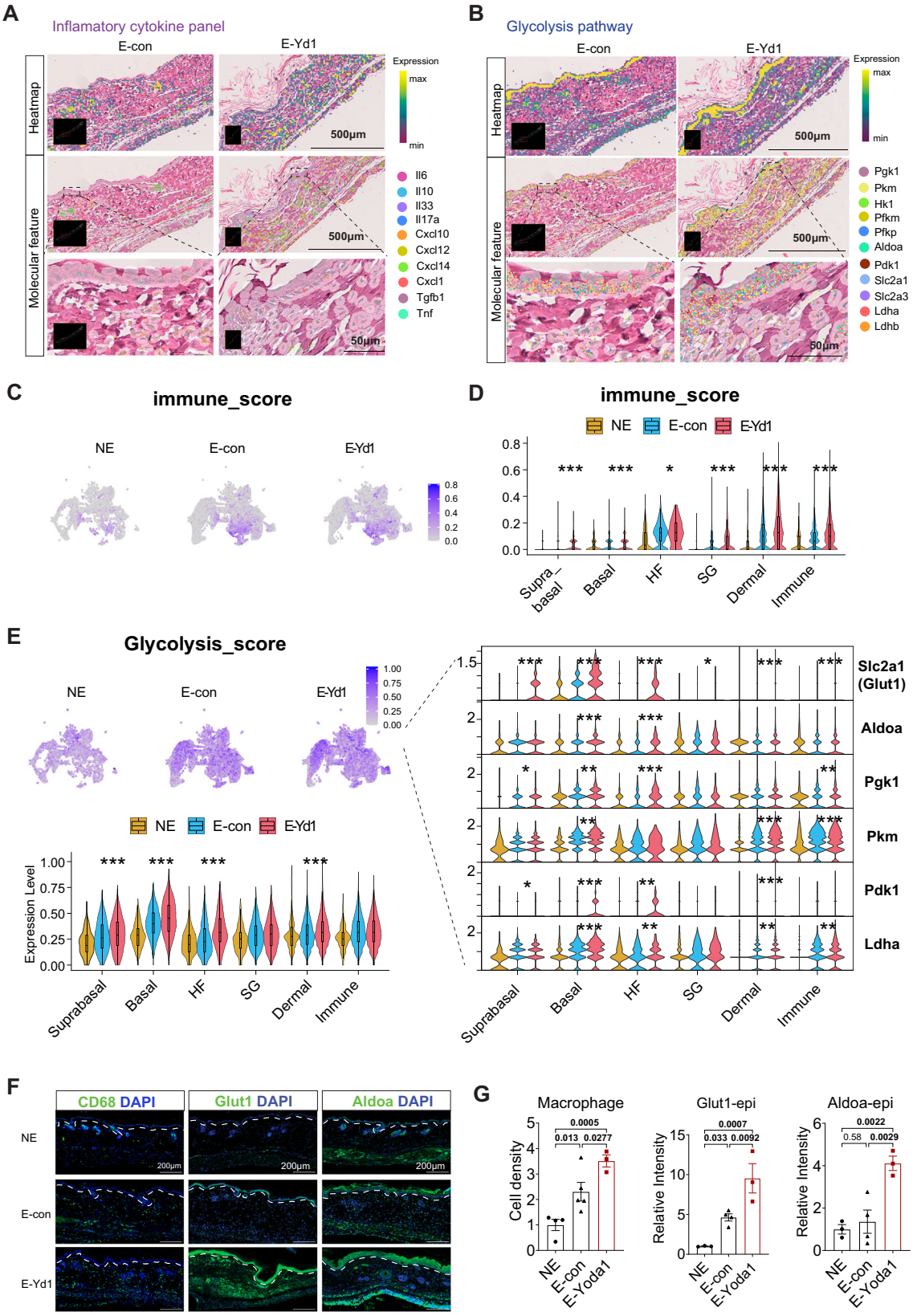

needed to understand Glut1's impact on tissue expansion. Aldolase is a crucial enzyme in the fourth step of glycolysis. It plays an essential role in keratinocyte migration during wound repair[53] and may function through the Aldoa/HIF-1α pathway[54]. Our research suggests that Piezo1 activation stimulates glucose intake and the activity of glycolytic enzymes in stretched cells to facilitate skin growth.

Research indicates that activating Piezo1 promotes glycolysis in macrophages through the Ca^{2+}-induced CaMKII-HIF1α axis[55]. HIF1α plays a crucial role in enhancing glycolysis in low-oxygen conditions[56]. Interestingly, we noticed an increase in the hypoxia pathway following tissue expansion. We observed elevated *Hif1α* gene expression levels in all cell types, which can be further enhanced by Piezo1 activation

Fig. 6 | Piezo1 activation increases the inflammation and glycolysis pathways. **A** upper: spatial heatmap of cytokine panel genes in E-con and E-Yd1 skin; middle: spatial plot of cytokines; lower: high-resolution spatial map of cytokines. **B** upper: spatial heatmap of glycolysis pathway in E-con and E-Yd1 skin; middle: spatial plot of glycolysis-related genes; lower: high-resolution spatial map of glycolysis genes. **C** The UMAP shows immune_score based on the expression of the cytokine panel list in (**A**). **D** The violin plot showed immune_scores across various cell types. **E** The upper left UMAP shows Glycolysis_score based on the expression of the gene panel list in Fig. 3C. The lower left violin plot showed Glycolysis_scores across various cell types among samples. The right violin plot shows the expression of the representative glycolysis genes in xenium clusters. Significant test results between E-con and E-Yd1 samples were labeled on the violin plot. Detailed comparison results can be found in supplementary datasets. **F**, **G** Immunofluorescence staining of macrophage marker CD68, and glycolysis markers Glut1 and Aldoa, followed by quantification. CD68 is quantified in the dermis, and Glut1 and Aldoa are quantified in the epidermis. (n = 3). In multivariate analyses, the one-way ANOVA test was used. Wilcoxon rank-sum test was used for all violin plots in this manuscript.

during TE (Fig. 5H, I). All of these findings suggest that tension-activated Piezo1 amplifies the response to microenvironmental hypoxia and triggers the rewiring of glucose metabolism.

After noticing negative changes in the insulin-stimulated glucose uptake pathway through single-cell sequencing, we were curious about the potential impact on global glucose metabolism due to local glucose metabolism changes. The results indicate that local skin expansion does not currently impair glucose metabolism or insulin activity, as might be expected if skin stretch were an independent variable worsening the metabolic syndrome in obesity. However, we did not observe defects in blood glucose homeostasis. We believe further studies are needed, such as testing a high-fat diet and later chronic time points, to see if TE effects may better elucidate systemic metabolic consequences of markedly enhanced skin volume such as seen in obesity.

Piezo1 as a central coordinator of inflammation and metabolism in TE

Evidence for a role of PIEZO in coordinating the biological response in tissue expansion is the close similarity between the known specific cohort functions of PIEZO and the cohort changes observed in TE. While we and others have separately noted the importance of inflammation and metabolism in tissue restoration, how they are coordinately promoted is less appreciated. As an important candidate for this coordination, PIEZO has been separately associated with metabolic and inflammatory functions, particularly in animal models. Activation of Piezo1 promotes glycolysis in macrophages[55]. When Piezo1 is activated through the intracellular accumulation of glucose metabolites, it triggers insulin secretion in pancreatic beta cells[57]. Additionally, Piezo1 may regulate diet-induced adipocyte inflammation and systemic glucose metabolism[58]. Piezo1 is abundant in mechano-active tissues such as the skin and the lung and is associated with innate and adaptive inflammatory responses[34,47,59]. In a study on mechanical force-induced stress in the skin, researchers demonstrated that knocking down Piezo1 in epidermal stem cells reduces immune activation pathways[35]. Therefore, in mice, PIEZO known functional role in inflammation and metabolism suggest it might be a candidate in TE given the overlapping gene expression changes in these pathways.

Therapeutic implications

The role of PIEZO1 in humans is not as well studied, but with some implications of these same functions. Most classically, Piezo1 mutations are associated with human pathologic conditions including gain of function mutations resulting in xerocytosis[23], and loss of functions associated with lymphadenopathy and hydrops fetalis[60]. Nevertheless, there are also limited but suggestive data linking Piezo1 to metabolic and inflammatory phenotypes in humans. A study found that GOF PIEZO1 is an important genetic factor involved in iron metabolism in individuals of non-European ancestry[61]. Notably, Piezo1 and key inflammatory biomarkers are highly expressed in the ileum of patients with active Crohn's disease[62]. Interestingly, novel large-scale GWAS associations mapping to PIEZO1 loci suggest underexplored connections to metabolism and inflammation (https://www.ebi.ac.uk/gwas/genes/PIEZO1) in humans. For example, the rs837763-T polymorphism in Piezo1 has a very significant association (2×10^{-117}) with Hgba1c levels, a marker of hyperglycemia. Other PIEZO1 loci are also significantly associated with Body Mass Index, such as rs4782429. Finally, rs475596 and others are associated with neutrophil and lymphocyte counts in the blood. These results suggest a potential role for PIEZO in metabolism and inflammation, also in humans.

The discovery of Piezo1's role in the coordination of skin growth in response to tension represents a significant advance. Our research showed that Piezo1 plays a crucial role in orchestrating tension-induced inflammation and metabolism modulation. The impaired skin growth observed in animals with defective epidermal-Piezo1, as well as the enhanced skin growth in animals treated with the Piezo1 activator Yoda1, underscores the functional significance of Piezo1. Several studies have shown that Yoda1 regulates wound healing or skin itching through epidermal-Piezo1[63]. In epidermal-Piezo1 knockout mice, both epidermal and dermal thickness are reduced, indicating that diminished epidermal growth affects overall skin growth and is interesting for further investigation. This finding highlights the close coordination between the epidermis and dermis during tissue restoration. The rapid growth of the epidermis appears to provide a foundation for the growth of the entire skin, emphasizing its critical role and offering valuable insights for designing future strategies to enhance tissue expansion. The finding of the Piezo1-YAP axis addresses the downstream biological network that Piezo1 initiates for skin growth. Interestingly, Piezo1 activation also links to inflammation changes[34], which is one of the tension-induced features in the skin. This knowledge can be harnessed to develop innovative approaches to facilitate skin growth and repair in tissue expansion for conditions like burns, trauma, or major skin defects or loss after surgery[2,3,10]. Leveraging the power of Piezo1 activators such as Yoda1[36] may enable safer and more efficacious tissue expansion than what is currently achieved with mechanical devices.

Summary

In conclusion, we discovered that tension activates piezo1 in the skin, which leads to increased skin growth, local inflammation, and reprogramming of metabolism (Fig. 7). By using a piezo1 activator, we accelerated these changes, suggesting a mechano-immune-metabolic axis that controls skin growth. Spatial transcriptomics mapped enriched inflammatory-metabolic activity in the TE skin to their cellular origins, offering a comprehensive understanding of the interactions within the stretched skin microenvironment under modified physical constraints.

Our discovery suggests the potential for non-surgical methods to promote skin growth. These insights imply advanced therapeutic interventions aimed at modulating inflammatory-metabolic pathways to enhance skin growth in clinical settings. Furthermore, our findings may also provide insight into developing targeted therapies for conditions involving skin stretch, dysregulated inflammation, and metabolism, such as obesity.

Methods

Mice

All mouse experiments were approved by the Johns Hopkins University Animal Care and Use Committee (IACUC) and abided by IACUC protocols (#MO23M262). Animals were maintained in the Johns Hopkins

https://doi.org/10.1038/s41467-025-62270-3

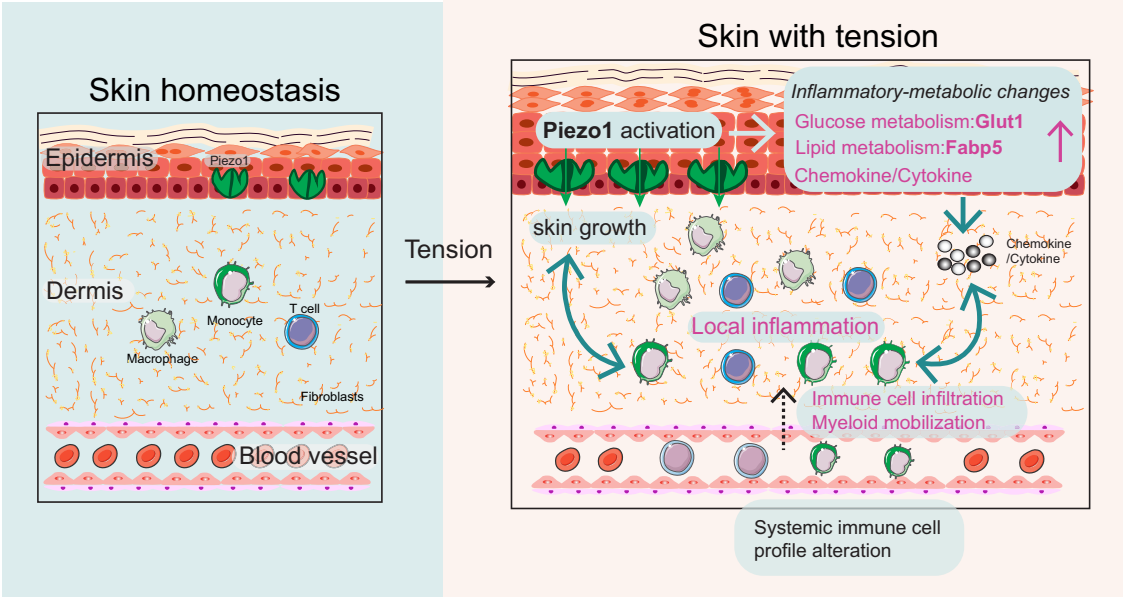

Fig. 7 | Graphical summary. Tension activates an inflammatory-metabolic molecular network in the skin, including inflammatory signal activation, immune cell infiltration, circulating myeloid cell mobilization, and metabolic changes. Piezo1 orchestrates stretch-induced skin growth, inflammation, and metabolic changes.

School of Medicine animal facilities. Animals were acclimated to the ambient conditions of the facilities (20–26 °C and 40–60% humidity) before the start of the experiments, allowed access to food and water, kept on a 12 h on/off light cycle. All mouse backgrounds are based on C57BL/6. DNA was extracted from the digit tips of young pups or the tail tip in adult mice, followed by PCR for genotyping. We use male mice for tissue expansion assay due to the size/weight difference between genders.

Piezo1 loss-of-function model. To delete Piezo1 protein specifically in Krt5^{+} epidermal stem cells in the skin, we crossed the Krt5-Cre^{ERT2} mice strain with the Piezo1^{flox} mice strain. The Krt5-Cre^{ERT2} mice were from Dr. Michael Caterina's lab at Johns Hopkins Medicine. The Piezo1^{flox} mice were from The Jackson Laboratory (# 029213). To induce gene knockout, the Krt5^{Cre};Piezo1^{flox} (K5;P1f) mice were treated with TAM intraperitoneally (100 mg/kg/day) five times a week for 1 week, followed by 3 times a week for another week (Fig. 4D).

Tissue expansion model protocol

Mice were anesthetized with volatile anesthesia (Baxter, Isoflurane). Using surgical scissors, a transverse cut was made into the dorsal skin below the neck of adult mice (8–9 weeks, around 24 g), allowing for the insertion of a silicone expander (PMT, catalog# 3611-376) subcutaneously on D0 (pre-injection). This incision was then sutured, and after allowing for 7 days of recovery, 4 mL of PBS was injected every 2 days for 12 days to achieve a total volume of 24 mL (Injection Day, I-0 – 10). For the control mice, expanders were implanted, but no PBS injections were administered, and subsequently, there was no applied mechanical stimulation. A 0.25 cm^2 square was marked on I-0 over the skin above the expander (E). The dimensions and mass of this square of tissue were measured throughout the expansion protocol. All procedures were performed under the biological safety cabinet of Johns Hopkins School of Medicine. All materials and reagents used are readily available from standard commercial companies.

Yoda1 treatment. Yoda1 was purchased from Sigma (SML1558). Yoda1 preparation. Yoda1 was diluted with DMSO to create a 40 mM stock solution, stored at −20 °C, and further PBS diluted to a 1 mM working solution for tissue expansion assay. We applied 1 mM * 10 µl (3.55 µg) Yoda1 in a 1 cm * 1 cm square of skin, which grows over the time of tissue expansion using the pipette tip. After application, spread the liquid over the area and remove excess liquid if necessary.

The Yoda1 treatment process in the tissue expansion assay included the following steps: Two days before inflating the tissue expander, Yoda1 was applied topically to the skin daily. On the day of the PBS injection to inflate the expander (I-0), four 0.5 × 0.5 cm marked areas were designated to monitor skin changes. Control expansion mice were left untreated. Skin size was measured every other day, with each square's size calculated as one-fourth of the total to minimize variation. Yoda1 was reapplied to these areas every other day until day four post-injection (PI-4), and skin samples were collected on day seven (PI-7). Yoda1 was diluted with DMSO to create a 40 mM stock solution, stored at −20 °C, and further diluted to a 10 mM working solution.

Skin sample collection

For Histology: Skin samples from mice were fixed in 4% paraformaldehyde overnight and then transferred to PBS. These biopsies were then sent to the Johns Hopkins Oncology Tissue Services Core facility to be embedded in paraffin, sectioned into 4 µm-thick segments, mounted onto glass slides, and stained with hematoxylin and eosin (H&E).

Flow cytometry

Skin Digestion. After euthanizing the mice, skin samples were collected from above the tissue expander in E and NE mice and placed in PBS on ice. Subcutaneous tissue was removed with forceps, and the skin was cut into pieces. Whole skin digestion solution [a mix of 0.25 mg/mL Liberase TL (ROCHE 05401020001) and 1 mg/mL DNase I ((Sigma DN25-1G)) was made in advance and kept on ice. The pieces were transferred to a digestion solution in a 6-well plate and incubated at 37 °C for 2 h. For the final 10 min, 1 mL of 0.25% Trypsin-1 mM EDTA (Gibco) was added. Digestion was stopped by adding 4 mL of cold 5% FACS buffer [PBS containing 5% fetal bovine serum (Sigma)]. The tissue was mechanically dissociated using a syringe with 8–10 gentle pumps, filtered through a 100 µm strainer, and centrifuged at 400 × *g* for 8 min at 4 °C. After washing and filtering again with 5% FACS buffer, cells were resuspended in FACS buffer for staining.

Flow cytometry staining[64]. Cells were stained with Zombie Aqua Fixable Viability Kit, followed by anti-mouse CD16/32 antibody (Fc block) and then stained with the designated antibody panel. After a 25-min incubation at 4 °C in the dark, cells were washed three times and kept on ice. Data were collected using an LSR Fortessa (BD Biosciences) and analyzed with FlowJo software.

Primary antibodies used are listed below. T-Myeloid Sorting Panel. Zombie Aqua™ Fixable Viability Kit (BioLegend, #423101, 1:200); PerCP/Cyanine5.5 anti-mouse CD45 (BioLegend, #103132, 1:100); FITC anti-mouse Lineage Cocktail with Isotype Control (BioLegend, #133302, 1:200); BUV395 anti-mouse Thy1.2 (CD90.2), clone 53-2.1 (BD Biosciences, #565257, 1:200); PE/Cyanine7 anti-mouse IL-17A (BioLegend, #506921, 1:100).

Myeloid Panel. FITC anti-mouse Lineage Cocktail (manually mixed): CD3e (BioLegend, #100306, 1:300), CD19 (BioLegend, #115506, 1:300), NK1.1 (BioLegend, #108706, 1:300), Siglec-F (BioLegend, #567005, 1:300); BUV395 anti-mouse/human CD11b (BD Biosciences, #565257, 1:200); Brilliant Violet 711™ anti-mouse Ly-6G/Ly-6C (Gr-1) (BioLegend, #108443, 1:200); APC anti-mouse CD64 (FcgRI) (BioLegend, #139306, 1:100); Brilliant Violet 421™ anti-mouse CD11c (BioLegend, #117329, 1:100); APC/Cyanine7 anti-mouse CD326 (EpCAM) (BioLegend, #118218, 1:100).

Blood cell collection and RNA-sequencing

Before collecting blood cells, the mice were anesthetized with isoflurane inhalation. blood was then collected by insert a sterile capillary tube into the retro-orbital sinus and allow blood to flow into it. The red blood cells were broken down using ACK buffer (Gibco), and the remaining PBMC cells were collected. These PBMC cells were then used to extract total RNA, which was submitted for sequencing.

Immunofluorescence staining

Skin tissue sections were first deparaffinized, after which heat-induced antigen retrieval was performed. After permeabilization in 0.2% Triton X-100 in TBS and washing in TBS, a blocking buffer (5% goat serum and 1% bovine serum albumin) was applied. For mouse-on-mouse (MOM) staining, unconjugated affinity-purified F(ab) fragment anti-mouse IgG (H + L) was applied and incubated for 1 h at room temperature to block endogenous IgG. Otherwise, the sections were then incubated with primary antibodies at 4 °C overnight. After additional washing, the samples were then incubated with secondary antibodies conjugated with fluorescent dye for 2 h at room temperature in the dark. After a final round of washing, the tissue sections were mounted with ProLong™ Gold Antifade Mountant with DAPI (Thermo Fisher, P36931). Primary antibodies used were as follows: anti-Ki67 (1:500; Abcam, ab15580; rabbit), anti-CD68 (1:100; Abcam, ab125212; rabbit), anti-Glut1 [1:200; Cell Signaling Technology (CST), #73015; rabbit], anti-Aldoa (rabbit, 1:100, abcam, ab252953, anti-YAP [rabbit; 1:100 for immunofluorescence, Cell Signaling Technology (CST), #14074T]). All tissue slides were imaged using fluorescence microscopy (Olympus VS200 Slide Scanner). Quantification was performed with ImageJ.

Microarray

According to the manufacturer's protocols, RNA samples isolated from mouse skin were submitted to the JHMI Deep Sequencing & Microarray core for Affymetrix® Human Exon 1.0ST and mouse microarray chip. Raw gene expression signals in the form of Affymetrix CEL files were extracted and normalized with Partek® Genomics SuiteTM software using the Robust Multichip Analysis (RMA) algorithm. Genes were ranked according to fold change of the intervention and referred to as top or bottom induced if they were at the highest fold change (top) or lowest fold change (bottom). Student's t-test analysis measured the significance of gene expression.

Single-cell RNA-seq

Cell isolation and live-cell selection. Skin samples were incubated in 0.4% Dispase II solution at 4 °C overnight. Epidermal sheets were separated from the dermis manually on the next day and digested in 0.25% trypsin/EDTA to obtain single cells[65]. Isolated cells were then stained with PI/DCV for flow cytometry sorting for single live cells in the flow cytometry core at the Johns Hopkins School of Public Health. PI-/DCV$^+$ single live cells were selected and submitted to JHMI Deep Sequencing & Microarray Core for single-cell sequencing.

Data preprocessing and quality control. We have two batches of data for a total of 4 samples, with each sample consisting of 3 biological replicates. After the initial cell ranger metric assessment, data were preprocessed with the Seurat package. We kept cells with more than 500 unique molecular identifiers (UMI), 200 genes, 0.7 cell complexity (log10GenePerUMI), and less than 0.1 mitochondria gene ratio and filtered out genes that were expressed in fewer than ten cells.

After quality control, 15,802 cells with 17,022 genes remained and were used for clustering. Briefly, single-cell data matrices were first normalized and log-transformed. Cell cycle phases were calculated and assigned using the software's CellCycleScoring function for each sample. To remove unwanted sources of variability caused by differences in cycling stages and mitochondrial ratio, we set the variable.features.n to be 3000 and included mitoRatio, S.scores, and G2/M.score in vars.to.regress. Next, to ensure that similar cells across the conditions were clustered, we used the top 3,000 highly variable genes for canonical correlation analysis implemented in Seurat to align and integrate the entire dataset. Principal component analysis was performed first, and the top 20 PCs (principal components) out of 40 pcs with resolution 0.45 were selected to obtain 16 clusters. By visualizing the established epithelial cell markers from the literature on the feature plot, we identified 13 clusters for downstream analysis. All details of the Seurat analyses performed in this work can be found in the website tutorial (https://satijalab.org/seurat/v3.0/pbmc3k_tutorial.html, https://github.com/hbctraining/scRNA-seq_online/tree/master/lessons).

Gene set enrichment analysis and gene ontology analysis. Gene ontology analysis of differentially expressed genes for pseudobulk data was performed by gprofiler2[66] (https://biit.cs.ut.ee/gprofiler/page/r). Representative terms were selected from top-ranked gene sets/pathways. All differentially expressed genes were first evaluated by the Wilcoxon rank-sum test (by function wilcoxauc in presto). The queried databases included MSigDB: CP: KEGG, CP: REACTOME, and Hallmark.

Spatial Xenium assay

Tissue preparation. Skin tissue samples were fixed with 4% PFA and embedded in paraffin. Sectioned slides amounted to xenium slides for downstream analysis. Adjacent sections were saved for HE staining. Post-xenium slides were also performed for the HE staining.

Data process. We followed the vignette from Satija Lab for data analysis (https://satijalab.org/seurat/articles/seurat5_spatial_vignette_2#mouse-brain-10x-genomics-xenium-in-situ). Cells from two repeated samples were combined.

Pathway gene list. All pathways gene lists are included in supplementary dataset 9. For the list of stretch-induced signature genes, the S100a8, Stfa1, Sprr2a3, Postn, Itgb1, and Gsdmc are from our previous microarray and publication, the Myh9, Diaph3, Stat3, and Ctnna1 are from published literature.

Statistics

All experiments were performed in at least three individual instances, unless otherwise noted. To perform univariate statistical analysis, the Student's t-test was used. For multivariate analyses, the one-way ANOVA test was used. Detailed comparison method was labeled in figure legend. Statistical significance was defined based on $p < 0.05$ (*), 0.01 (**), 0.001 (***) or 0.0001 (****), either p-value or the defined results were marked in the figures. Data are represented as Mean ± SEM. No statistical method was used to predetermine sample size. No data were excluded from the analysis. The statistics test results of the Xenium assay are stored in supplementary datasets 2–8.

Reporting summary

Further information on research design is available in the Nature Portfolio Reporting Summary linked to this article.

Data availability

The microarray and single-cell sequencing data generated in this study have been deposited in NCBI's Gene Expression Omnibus database under accession code GSE186774. The xenium data generated in this study have been deposited in NCBI's Gene Expression Omnibus database under accession code GSE289263. Source data are provided with this paper.

References

1. Sachs, D. et al. Sustained physiological stretch induces abdominal skin growth in pregnancy. *Ann. Biomed. Eng.* **52**, 1576–1590 (2024).
2. Wagh, M. S. & Dixit, V. Tissue expansion: concepts, techniques and unfavourable results. *Indian J. Plast. Surg.* **46**, 333–348 (2013).
3. Radovan, C. Tissue expansion in soft-tissue reconstruction. *Plast. Reconstr. Surg.* **74**, 482–492 (1984).
4. De Filippo, R. E. & Atala, A. Stretch and growth: the molecular and physiologic influences of tissue expansion. *Plast. Reconstr. Surg.* **109**, 2450–2462 (2002).
5. Takei, T., Mills, I., Arai, K. & Sumpio, B. E. Molecular basis for tissue expansion: clinical implications for the surgeon. *Plast. Reconstr. Surg.* **102**, 247–258 (1998).
6. Chu, S. Y. et al. Mechanical stretch induces hair regeneration through the alternative activation of macrophages. *Nat. Commun.* **10**, 1524 (2019).
7. Adler, N., Dorafshar, A. H., Bauer, B. S., Hoadley, S. & Tournell, M. Tissue expander infections in pediatric patients: management and outcomes. *Plast. Reconstr. Surg.* **124**, 484–489 (2009).
8. Antonyshyn, O., Gruss, J. S., Mackinnon, S. E. & Zuker, R. Complications of soft tissue expansion. *Br. J. Plast. Surg.* **41**, 239–250 (1988).
9. Manders, E. K. et al. 3rd. Soft-tissue expansion: concepts and complications. *Plast. Reconstr. Surg.* **74**, 493–507 (1984).
10. Razzak, M. A. et al. Cellular and molecular responses to mechanical expansion of tissue. *Front. Physiol.* **7**, 540 (2016).
11. Xue, Y. et al. Mechanical tension mobilizes Lgr6(+) epidermal stem cells to drive skin growth. *Sci. Adv.* **8**, eabl8698 (2022).
12. Wang, Z. et al. Metabolic reprogramming in skin wound healing. *Burns Trauma* **12**, tkad047 (2024).
13. Konieczny, P. et al. Interleukin-17 governs hypoxic adaptation of injured epithelium. *Science* **377**, eabg9302 (2022).
14. Brandao, A. S. et al. A regeneration-triggered metabolic adaptation is necessary for cell identity transitions and cell cycle re-entry to support blastema formation and bone regeneration. *Elife* **11**, e76987 (2022).
15. Wang, G. et al. Bacteria induce skin regeneration via IL-1beta signaling. *Cell Host Microbe* **29**, 777–791 e6 (2021).
16. Xue, Y., Reddy, S. K. & Garza, L. A. Toward understanding wound immunology for high-fidelity skin regeneration. *Cold Spring Harb. Perspect. Biol.* **14**, a041241 (2022).
17. Naik, S. et al. Inflammatory memory sensitizes skin epithelial stem cells to tissue damage. *Nature* **550**, 475 (2017).
18. Nelson, A. M. et al. dsRNA released by tissue damage activates TLR3 to drive skin regeneration. *Cell Stem Cell* **17**, 139–151 (2015).
19. Marchioro, H. Z. et al. Update on the pathogenesis of vitiligo. *Bras. Dermatol.* **97**, 478–490 (2022).
20. Aragona, M. et al. Mechanisms of stretch-mediated skin expansion at single-cell resolution. *Nature* **584**, 268–273 (2020).
21. Ding, J. et al. Macrophages are necessary for skin regeneration during tissue expansion. *J. Transl. Med.* **17**, 36 (2019).
22. Liu, W. et al. Transcriptome profiling reveals important transcription factors and biological processes in skin regeneration mediated by mechanical stretch. *Front. Genet.* **12**, 757350 (2021).
23. Coste, B. et al. Piezo1 and Piezo2 are essential components of distinct mechanically activated cation channels. *Science* **330**, 55–60 (2010).
24. Mikesell, A. R. et al. Keratinocyte PIEZO1 modulates cutaneous mechanosensation. *Elife* **11**, e65987 (2022).
25. Xie, Y. et al. Hair shaft miniaturization causes stem cell depletion through mechanosensory signals mediated by a Piezo1-calcium-TNF-alpha axis. *Cell Stem Cell* **29**, 70–85.e6 (2022).
26. Hayes, J. & Higgins, C. A. Plantar skin: a callus design?. *J. Investig. Dermatol.* **144**, 1427–1429 (2024).
27. Wang, Y. et al. Functional regeneration and repair of tendons using biomimetic scaffolds loaded with recombinant periostin. *Nat. Commun.* **12**, 1293 (2021).
28. Protter, D. S. W. & Parker, R. Principles and properties of stress granules. *Trends Cell Biol.* **26**, 668–679 (2016).
29. Jin, S. et al. Inference and analysis of cell-cell communication using CellChat. *Nat. Commun.* **12**, 1088 (2021).
30. Xue, Y. et al. Mechanical tension mobilizes Lgr6+ epidermal stem cells to drive skin growth. *Sci. Adv.* **8**, eabl8698 (2022).
31. Rohm, T. V., Meier, D. T., Olefsky, J. M. & Donath, M. Y. Inflammation in obesity, diabetes, and related disorders. *Immunity* **55**, 31–55 (2022).
32. Pearah, A. et al. Blocking AMPKalphaS496 phosphorylation improves mitochondrial dynamics and hyperglycemia in aging and obesity. *Cell Chem. Biol.* **30**, 1585–1600.e6 (2023).
33. Liu, H. et al. Piezo1 channels as force sensors in mechanical force-related chronic inflammation. *Front. Immunol.* **13**, 816149 (2022).
34. Atcha, H. et al. Mechanically activated ion channel Piezo1 modulates macrophage polarization and stiffness sensing. *Nat. Commun.* **12**, 3256 (2021).
35. Huang, S. et al. Stress vesicles are induced by acute mechanical force and precede the commitment of epidermal stem cells to terminal differentiation. *biorxiv*. https://doi.org/10.1101/2022.09.29.510204 (2022).
36. Ma, N. et al. Piezo1 regulates the regenerative capacity of skeletal muscles via orchestration of stem cell morphological states. *Sci. Adv.* **8**, eabn0485 (2022).
37. Mascharak, S. et al. Preventing Engrailed-1 activation in fibroblasts yields wound regeneration without scarring. *Science* **372**, eaba2374 (2021).
38. Chen, K. et al. Disrupting mechanotransduction decreases fibrosis and contracture in split-thickness skin grafting. *Sci. Transl. Med.* **14**, eabj9152 (2022).
39. Frank, S., Stallmeyer, B., Kampfer, H., Kolb, N. & Pfeilschifter, J. Leptin enhances wound re-epithelialization and constitutes a direct function of leptin in skin repair. *J. Clin. Investig.* **106**, 501–509 (2000).
40. Shibata, S. et al. Adiponectin regulates cutaneous wound healing by promoting keratinocyte proliferation and migration via the ERK signaling pathway. *J. Immunol.* **189**, 3231–3241 (2012).

41. D'Esposito, V. et al. Adipocyte-released insulin-like growth factor-1 is regulated by glucose and fatty acids and controls breast cancer cell growth in vitro. *Diabetologia* **55**, 2811–2822 (2012).
42. Ogawa, R. et al. The relationship between skin stretching/contraction and pathologic scarring: the important role of mechanical forces in keloid generation. *Wound Repair Regen.* **20**, 149–157 (2012).
43. Chen, K. et al. Mechanical strain drives myeloid cell differentiation toward proinflammatory subpopulations. *Adv. Wound Care* **11**, 466–478 (2022).
44. Ledwon, J. K., Kelsey, L. J., Vaca, E. E. & Gosain, A. K. Transcriptomic analysis reveals dynamic molecular changes in skin induced by mechanical forces secondary to tissue expansion. *Sci. Rep.* **10**, 15991 (2020).
45. Theocharidis, G. et al. A strain-programmed patch for the healing of diabetic wounds. *Nat. Biomed. Eng.* **6**, 1118–1133 (2022).
46. Meli, V. S. et al. YAP-mediated mechanotransduction tunes the macrophage inflammatory response. *Sci. Adv.* **6**, eabb8471 (2020).
47. Du, H. et al. Tuning immunity through tissue mechanotransduction. *Nat. Rev. Immunol.* **23**, 174–188 (2023).
48. Shutova, M. S. & Boehncke, W. H. Mechanotransduction in skin inflammation. *Cells* **11**, 2026 (2022).
49. Zhang, P. et al. Tenascin-C can serve as an indicator for the immunosuppressive microenvironment of diffuse low-grade gliomas. *Front. Immunol.* **13**, 824586 (2022).
50. Pakshir, P. et al. Dynamic fibroblast contractions attract remote macrophages in fibrillar collagen matrix. *Nat. Commun.* **10**, 1850 (2019).
51. Zhang, Z. et al. Differential glucose requirement in skin homeostasis and injury identifies a therapeutic target for psoriasis. *Nat. Med.* **24**, 617–627 (2018).
52. Cibrian, D., de la Fuente, H. & Sanchez-Madrid, F. Metabolic pathways that control skin homeostasis and inflammation. *Trends Mol. Med.* **26**, 975–986 (2020).
53. Tochio, T., Tanaka, H., Nakata, S. & Hosoya, H. Fructose-1,6-bisphosphate aldolase A is involved in HaCaT cell migration by inducing lamellipodia formation. *J. Dermatol. Sci.* **58**, 123–129 (2010).
54. Liu, Y. et al. Adipose-derived mesenchymal stem cell-loaded beta-chitin nanofiber hydrogel activates the AldoA/HIF-1alpha pathway to promote diabetic wound healing. *Am. J. Stem Cells* **12**, 1–11 (2023).
55. Leng, S. et al. Ion channel Piezo1 activation promotes aerobic glycolysis in macrophages. *Front. Immunol.* **13**, 976482 (2022).
56. Urrutia, A. A. et al. HIF1alpha-dependent uncoupling of glycolysis suppresses tumor cell proliferation. *Cell Rep.* **43**, 114103 (2024).
57. Ye, Y. et al. A critical role of the mechanosensor PIEZO1 in glucose-induced insulin secretion in pancreatic beta-cells. *Nat. Commun.* **13**, 4237 (2022).
58. Zhao, C. et al. Mechanosensitive ion channel Piezo1 regulates diet-induced adipose inflammation and systemic insulin resistance. *Front. Endocrinol.***10**, 373 (2019).
59. Targeting the PIEZO1 pathway boosts T cell antitumour cytotoxicity. *Nat. Biomed. Eng*. https://doi.org/10.1038/s41551-024-01189-4 (2024).
60. Fotiou, E. et al. Novel mutations in PIEZO1 cause an autosomal recessive generalized lymphatic dysplasia with non-immune hydrops fetalis. *Nat. Commun.* **6**, 8085 (2015).
61. Ma, S. et al. A role of PIEZO1 in iron metabolism in mice and humans. *Cell* **184**, 969–982.e13 (2021).
62. Liu, Q. Y. et al. The mechanosensitive ion channel PIEZO1 in intestinal epithelial cells mediates inflammation through the NOD-like receptor 3 pathway in Crohn's disease. *Inflamm. Bowel Dis.* **29**, 103–115 (2023).
63. Holt, J. R. et al. Spatiotemporal dynamics of PIEZO1 localization controls keratinocyte migration during wound healing. *Elife* **10**, e65415 (2021).
64. Sakamoto, K., Goel, S., Funakoshi, A., Honda, T. & Nagao, K. Flow cytometry analysis of the subpopulations of mouse keratinocytes and skin immune cells. *STAR Protoc.* **3**, 101052 (2022).
65. Lim, C. H. et al. Hedgehog stimulates hair follicle neogenesis by creating inductive dermis during murine skin wound healing. *Nat. Commun.* **9**, 4903 (2018).
66. Raudvere, U. et al. g:Profiler: a web server for functional enrichment analysis and conversions of gene lists (2019 update). *Nucleic Acids Res.* **47**, W191–W198 (2019).

Acknowledgements

We thank Y. Xuan of the JHU SKCCC Core for helping us with the flow cytometry experiments; R. Hughes, L. Orzolek, and C. Talbot at the Johns Hopkins Transcriptomics and Deep Sequencing Core with the microarray and single-cell sequencing, and spatial xenium assays. We acknowledge the assistance of the Servier Medical Art for providing resources used in the Fig. 7 graphic illustrations. Specifically, the immune cells and blood vessels used in Fig. 7 are from Servier Medical Art under the Creative Commons Attribution 4.0 International License (CC BY 4.0). Research reported in this publication was supported by the National Institute of Arthritis and Musculoskeletal and Skin Diseases, part of the National Institutes of Health (NIH), under R01 AR074846 and R56 AR082660 to L.A.G., as well as the Daniel Nathans Scholar fund to L.A.G.; the Maryland Stem Cell Research Fund Award 2022-MSCRFD-5917 and sub-award under NIH National Institute on Aging #P30AG 021334 to S.K.R. and Dermatology Foundation Research Career Development Award to Y.X..

Author contributions

Conceptualization: L.A.G., S.K.R., and Y.X. Methodology: L.A.G., S.K.R., Y.X., Z.Z, I.L., S.W., C.K., S.L., A.L., K.W., C.L., K.Y., and L.H., Investigation: Y.X., E.W., Z.Z, I.L. and C.L., Visualization: Y.X. E.W., Z.Z., I.L., and H.M., Funding acquisition: L.A.G., S.K.R. and Y.X., Project administration: L.A.G., S.K.R. and Y.X., Supervision: L.A.G., S.K.R. and L.H., Writing—original draft: L.A.G., S.K.R. and Y.X., Writing—review and editing: L.A.G., S.K.R., E.W., and Y.X.

Competing interests

L.A.G. has received grant support paid to his institution, Johns Hopkins University from Sun Pharma Advanced Research Company (SPARC). This grant is to investigate intellectual property where Johns Hopkins University is the owner, L.A.G. is one of several inventors, is under a licensing agreement with SPARC, and has resulted in royalty payments to inventors. This grant and royalty payments are not related to the research presented in this manuscript. The remaining authors declare no competing interests.

Additional information

Supplementary information The online version contains supplementary material available at https://doi.org/10.1038/s41467-025-62270-3.

Correspondence and requests for materials should be addressed to Yingchao Xue, Sashank K. Reddy or Luis A. Garza.

Peer review information *Nature Communications* thanks Kellen Chen and the other, anonymous, reviewer for their contribution to the peer review of this work. A peer review file is available.